Available online at www.sciencedirect.com
ScienceDirect
Journal of the European Ceramic Society 27 (2007) 3561–3572
www.elsevier.com/locate/jeurceramsoc

Short-fibre-reinforced reaction-bonded silicon nitride (RBSN) by precursor route: Processing and properties

A. Herzog [a,*], G. Woetting [b], U.F. Vogt [a]

[a] *Department of High Performance Ceramics, Swiss Federal Laboratories for Materials Testing and Research (EMPA), Ueberlandstr. 129, CH-8600 Duebendorf, Switzerland*
[b] *H. C. Starck Ceramics GmbH & Co. KG, Lorenz-Hutschenreuther-Strasse 81, 95100 Selb, Germany*

Received 7 January 2006; received in revised form 26 July 2006; accepted 7 August 2006
Available online 19 April 2007

Abstract

A new approach to manufacture short-fibre-reinforced ceramic matrix composites (CMC) by mixing carbon fibres, ceramic fillers and a viscous ceramic precursor by means of a plastic forming technique is introduced. To transform the composite from the polymer into a nitride ceramic state, a two-step process consisting of pyrolysis and nitridation is applied. Transformations of the polymer-modified RBSN (PMRBSN) during this process are examined in terms of dimensional changes, porosity and phase composition. The role of the precursor during the processing and nitridation sequence, aspects concerning fibre shortening and packing and the effects on the material properties as Young's modulus, strength, hardness, porosity, crack deflection and fibre pullout are discussed.

Keywords: Short fibre reinforcement; Composites; Precursors-organic; Mixing; Pressing; Si_3N_4

1. Introduction

Fibre reinforcement of ceramics is an interesting approach applied to increase their toughness, strength, reliability, and damage tolerance. However, over the past decade only long fibre reinforced CMC's have successfully established themselves in practical applications. Their high cost, caused by the need to use the manual filament winding technique, allow only applications in cost-tolerant branches like the defence and aerospace industries. In order to open the advantages of fibre reinforced ceramics to a broader field of applications, efforts are being made to lower these fabrication costs. One of the possibilities being pursued is the use of short-fibre reinforcements.

Up to now primarily the liquid silicon infiltration route has been applied to fabricate short-fibre CMC's[1] and in brake applications these composites have already achieved a certain commercial success.[2,3] However, the temperatures up to 1600 °C applied during infiltration of liquid silicon into ceramic structures cause severe problems with respect to the structural integrity of ceramic fibres. Consequently, only carbon fibres are used in such CMC's, and this demands additionally that the whole CMC be protected against oxidation and thus limits its applications regarding temperature and atmosphere significantly.

Here, a new concept has been developed to obtain short-fibre-reinforced CMC's, namely by mixing fibres, ceramic fillers and a viscous ceramic precursor and then forming this mixture into the desired shape. For this approach the concept of active filler pyrolysis (AFCOP)[4] was utilised, where the volume expansion of the nitridation reaction is used to achieve pore closure and the polymer introduction is used to allow cost-effective plastic forming techniques. The relatively low temperatures needed for nitridation allow the use of more temperature sensitive ceramic fibres.

2. Experimental procedure

Mixing of C-fibres (Sigrafil C25, SGL Carbon), preceramic polymer (NH2100, Huels), Si_3N_4 (LC10N, H.C. Starck) and silicon (Bayer) was performed over a period of 2 h in a heated kneader (Werner&Pfleiderer, Luk 8.0). Subsequently the material was cooled down, granulated and formed into discs by warm pressing at 10 MPa, 150 °C (WirtzBuehler, Simplimet 2000).

* Corresponding author.
E-mail address: andreas.herzog@heraeus.com (A. Herzog).

0955-2219/$ – see front matter © 2007 Published by Elsevier Ltd.
doi:10.1016/j.jeurceramsoc.2006.08.021

Table 1
Specimen composition

Specimen	Fibre	Composition (wt%)				Composition (vol%)			
		Fibre	Si	NH 2100	Si_3N_4	Fibre	Si	NH 2100	Si_3N_4
A0	None	0	71.5	28.5	0	0	58.3	41.7	0
A2	Carbon	30	41.5	28.5	0	29.6	31.6	38.9	0
A3	Carbon	40	31.5	28.5	0	38.5	23.4	38.0	0
B0	None	0	42.9	28.5	28.6	0	37.4	44.5	18.1
B2	Carbon	30	24.9	28.5	16.6	30.6	19.6	40.3	9.5
X2	Carbon	20	42.5	37.5	0	19.0	31.6	49.4	0

The pressed discs (diameter 50 mm) were cured in air while heating up to 235 °C at a rate of 1 K/h and then cut into bars of 4 mm × 8 mm × 20–50 mm by using a diamond saw. The examined compositions are summarised in Table 1.

Pyrolysis was carried out in flowing nitrogen (1 l/min, purity 99.999) in an Al_2O_3-tube furnace (Gero HTK) with program "T0":

$$\text{T0}: \text{RT} \rightarrow 160\,^{\circ}\text{C}\ (160\,\text{K/h}) \rightarrow 750\,^{\circ}\text{C}\ (20.4\,\text{K/h}) \rightarrow 900\,^{\circ}\text{C}\ (42.8\,\text{K/h}),\quad p_{N_2} = 0.1\,\text{MPa},\ \text{pyrolysis}$$

This was followed by nitridation at different nitrogen pressures and peak temperatures ("T1": 0.1 MPa, 1400 °C and "T3": 9.5 MPa, 1310 °C):

$$\text{T1}: \text{RT} \rightarrow 1170\,^{\circ}\text{C}\ (180\,\text{K/h}) \rightarrow 1400\,^{\circ}\text{C}\ (9.6\,\text{K/h}),\ 24\,\text{h holding},\quad p_{N_2} = 0.1\,\text{MPa},\ \text{nitridation}$$

$$\text{T3}: \text{RT} \rightarrow 1170\,^{\circ}\text{C}\ (323\,\text{K/h}) \rightarrow 1310\,^{\circ}\text{C}\ (28\,\text{K/h}),\ 5\,\text{h holding},\quad p_{N_2} = 9.5\,\text{MPa},\ \text{nitridation}$$

Development of the phase composition was studied by powder diffraction (Philips PW 1710) in combination with external Si_3N_4 and Si_2ON_2 standards to enable quantification. The SiC content was calculated from the total carbon content, Eq. (1), which was determined using a carbon detector (CSA 2003, Leybold-Heraeus) via oxidation to CO_2 and detection by an IR sensor. Free silicon was determined by a gas volumetric method via disintegration with soda and hydrogen development according to DIN 51075. Free carbon content was identified by oxidation for 1 h at 1000 °C, where oxidation of the phases SiC, Si_3N_4 and Si_2ON_2 is almost negligible. To make a comparison between the carbon content before and after nitridation, possible weight changes due to nitridation had to be taken into consideration and the carbon content after nitridation was corrected by Eq. (2). For further information regarding these analysis methods, refer to Herzog.[5] Due to the presence of amorphous phases within the specimens, which mainly stem from the ceramised polymer, the content of crystallised phases never reached 100 wt%.

$$\text{wt\%(SiC)} = (\text{wt\%}(C_{\text{total}})) - (\text{wt\%}(C_{\text{free}})) \times 3.3 \quad (1)$$

$$\text{wt\%}(C_{\text{before nit.}}) = \text{wt\%}(C_{\text{after nit.}}) \times (1 + \Delta\text{wt\%}(C_{\text{due to nit.}})) \quad (2)$$

The specimens were also characterised by optical microscopy (Zeiss) and by scanning electron microscope Joel JSM 6000 after sputtering coating with Au/Pt. Open porosity was measured using a mercury porosimeter (Micromeritics, Autopore II 9220). Changes in skeletal density of the precursor during pyrolysis were determined with a helium pycnometer. Changes in length were analysed using dilatometry (402E, Netzsch), where samples were heated at 5 K/min up to 1170 °C and 2 K/min up to 1400 °C with a final holding time of 10 h. To allow comparison of the dimensional changes experienced by the samples during the different nitridation programs, the length changes of the samples were measured between the process steps by using a micrometer.

The strength of the nitrided specimens was determined in the 'as-fired' state in a 3-point bending test according to EN843-1 an Instron, Type 1362 universal testing machine with a crosshead speed of 1 mm/min.

A post-processing porosity reduction step involving infiltration of nitrided samples was done with a 50 wt% polysiloxane/hexane solution. For infiltration the samples were placed under vacuum, infiltrated with the solution and finally left to dry at atmospheric pressure. After drying the polymer was pyrolysed at 1300 °C for 4 h after heating at a rate of 110 K/h. After this pyrolysis further infiltration steps were performed according to the described procedure.

Young's modulus was measured with a 25 MHz ultrasonic source in water. From the dissemination speeds of the longitudinal (v_{long}) and transversal waves (v_{trans}), the transversal contraction number ϑ was determined and the Y-modulus calculated by Eq. (3).[6] These Y-moduli were only considered for data interpretation purposes if the deviation of the values within the same specimen was less than 5%.

$$E = \rho \times 10^{-3}(1 + \vartheta) + (1 - 2\vartheta) + \frac{v_{\text{long}}^2}{1 - \vartheta} \quad (3)$$

ϑ—transversal contraction $= \frac{2-(v_{\text{long}}/v_{\text{trans}})^2}{2-2\times(v_{\text{long}}/v_{\text{trans}})^2}$, ρ—density and v—dissemination speed of ultrasonic wave.

Vickers Hardness (HV10) was determined by the diamond pyramid method according to DIN 50133 using a Buehler PT-M-HV2 hardness testing machine. The crosshead speed of the diamond pyramid into the specimen surface was fixed at 100 μm/s up to a load of 98.07 N (10 kp) and the load was maintained for 25 s. The projected diagonal lengths d_1 and d_2 of the pyramid imprint were measured and hardness calculated according to DIN 55133.

3. Results

3.1. Green sample preparation

During mixing of the preceramic polymer with the silicon powder and the carbon fibres, a viscous paste is formed. Even at 38.5 vol% fibre content (A3), the paste is dominated optically by the matrix constituents. The fibres and the matrix constituents are well distributed. Increasing the polymer content up to 49.4 vol% (X2) allows shaping of the mixtures by injection moulding. All batches containing less polymer (A and B series) are only shapeable by warm pressing (Fig. 1).

Extensive fibre shortening caused during mixing and granulating can be observed by optical light microscopy after the matrix is dissolved away by an organic solvent. An average fibre length of 190 μm is found after 60 min of mixing and after a further 60 min of mixing this drops to 120 μm. The volumetric fibre content has a negligible influence on this fibre shortening phenomenon. According to O'Conner,[7] fibre shortening is caused by shear forces introduced by the kneading blades.

The shear forces in the mixer also introduce observable fibre orientation in the material. In the slit between kneading blades and the walls of the kneader chamber, the fibres orient due to the forced laminar flow of the viscous matrix.[8] This orientation is frozen during cooling and preserved during granulation and warm pressing since the flow distance of the granulated material in the pressing die is to low. Therefore, areas of oriented fibres sized between 0.1 and 2 mm stemming from the granules can be found in the pressed discs, and the result is a so-called domain structure (Fig. 2).[9] The boundaries of the former granules are well-connected and can therefore only be identified by the areas of oriented fibres.

3.2. Pyrolysis

During pyrolysis thermal depolymerisation of the polysiloxane to form a Si-O-C ceramic takes place as described by different authors.[10–15] Pyrolysis is characterised by an increase in density ($1.3 \rightarrow 2.33\ \mathrm{g/cm^3}$) combined with a weight loss of 15 wt%, which causes significant volume shrinkage in excess of 50% of the preceramic phase. The linear shrinkage of the composite during pyrolysis $\varepsilon^{\mathrm{pf},0}$ can be calculated from the volume contents of polymer and filler material (inert up to pyrolysis temperature of 950 °C) according to a model developed by Greil and Seibold.[16]

$$\varepsilon^{\mathrm{pf},0} = (1 + \psi^{\mathrm{pf},0})^{1/3} - 1 \tag{4a}$$

$$\psi^{\mathrm{pf},0} = (1 - \alpha\beta)(1 - \zeta^0)V_{\mathrm{p}} \tag{4b}$$

$\psi^{\mathrm{pf},0}$ is volume shrinkage, V_{p} volume precursor, α (ceramic yield of precursor) = $(\mathrm{wt_{start}} - \mathrm{wt_{end}(T)})/(\mathrm{wt_{start}})$, β (quotient density) = $\rho_{\mathrm{start}}/\rho_{\mathrm{aus}(T)}$ and ζ^0 is open porosity.

The parameters α and β must be determined for the precursor and are summarised for the whole range of pyrolysis temperatures in Table 2. Open porosity ζ^0 is not taken into consideration for the calculation of shrinkage since open porosity of the pure matrix sample A0 is always under 5 vol% up to 900 °C (Fig. 3).

The dilatometry results for the fibreless A0 sample are in good accordance with the calculations, while for fibre reinforced sample A2 a difference between calculated and measured shrinkage at temperatures above 700 °C is found (Fig. 4). Below this temperature, specifically in the range 600–700 °C, crack formation

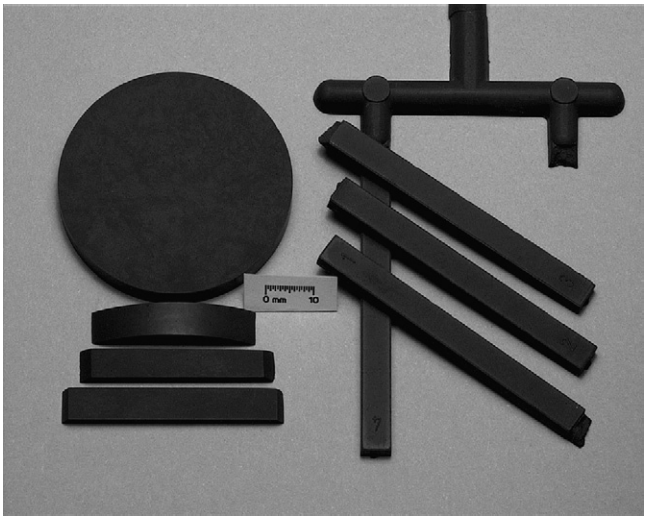

Fig. 1. Pressed (left, A2) and injection-moulded (right, X2) C-fibre composites after curing.

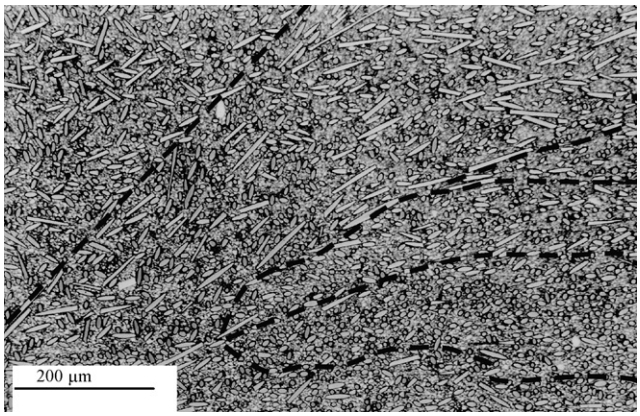

Fig. 2. Cross-section of A2 in the green state after pressing, areas of oriented fibres are separated by dotted lines (domain structure).

Table 2
Ceramic yield α and density quotient β of the precursor during pyrolysis

Temperature (°C)	α	β
230	1.0	1.0
500	1.0	0.9924
580	0.980	0.9924
600	0.975	0.9924
620	0.970	0.9924
650	0.965	0.9630
700	0.960	0.9091
750	0.870	0.8553
800	0.860	0.7429
850	0.850	0.6701
900	0.850	0.6075
950	0.850	0.5778

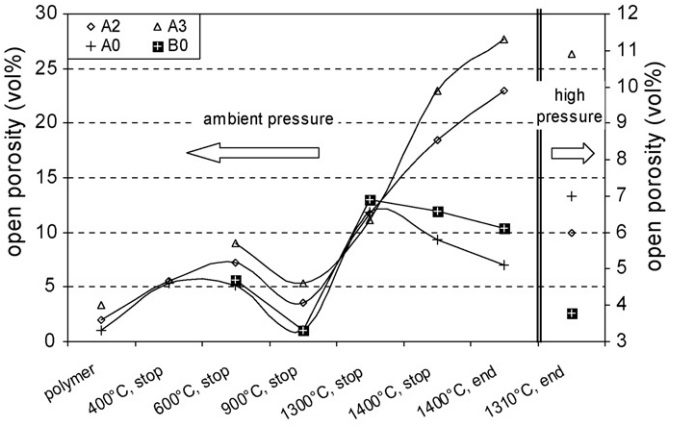

Fig. 3. Development of open porosity in different composites during pyrolysis and nitridation.

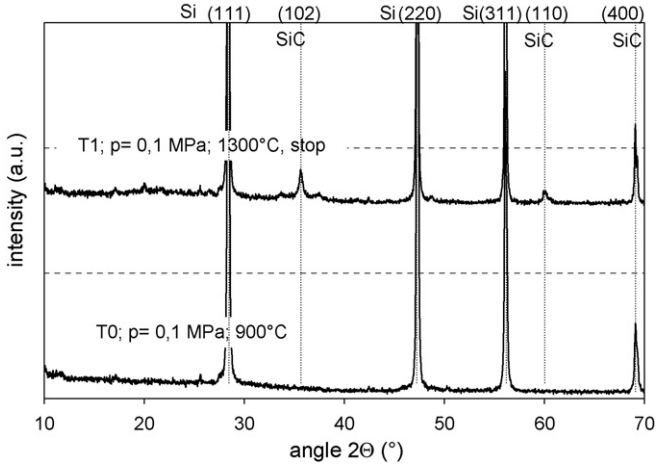

Fig. 5. X-ray spectra of specimen A0 after pyrolysis (T0) and nitridation (T1, stop at 1300 °C).

is observed to occur in the fibre containing samples. Cracks develop along the domains as described in Fig. 2 and propagate along the former granule boundaries during pyrolysis. Above 750 °C no further crack growth or development of new cracks are observed. In contrast to A2 and A3, the fibreless sample A0 shrinks without crack formation during the whole pyrolysis process.

As can be seen in Table 2, the ceramic yield α of the pure polymer is 85% after pyrolysis is finished at 900 °C. In combination with silicon and/or fibres and Si_3N_4 the ceramic yield of the precursor increases to 90% in accordance with the share of polymer in the whole composite. Thus, losses during pyrolysis of the polymer are cut down by 30%, which also has an influence on the shrinkage of the composites. Differences between different composite compositions are negligible. According to Erny et al.,[17] dissociation and adsorption of gaseous species CH_x, which split off during pyrolysis, on the surface of the reactive filler phase are responsible for the observed increase. For a titanium-vinylmethylphenylsiloxane mixture, Erny determined a 10 wt% greater precursor yield compared to the yield after pyrolysis of the pure precursor.

When pyrolysis is complete the polysiloxane is completely X-ray amorphous. For the silicon–polysiloxane mixture A0, silicon is found after pyrolysis to 900 °C (Fig. 5). Renlund et al.[10] first described the polysiloxane structure as a SiO_xC_y-glass built mainly of SiO_4 tetrahedra where the oxygen is partially substituted by carbon. Precipitation of clusters of turbostratic carbon within the amorphous SiOC is also observed.[18] Carbon analysis shows that all the carbon at this stage of pyrolysis, which stems from the precursor exists in the form of free carbon accessible for oxidation at 1000 °C (Fig. 6). However, according to Renlund et al.,[10] carbon from the pure polymer should be captured in the glass structure and therefore be impossible to access in significant amounts for oxidation. Stability of the carbon clusters against oxidation could be confirmed for the pure pyroylsed polymer by oxidation at 1000 °C. However, Müller[19] observed access to free carbon after pyrolysis of a $MoSi_2$–polysiloxane mixture by oxidation. Müller concluded that the different microstructure of the precursor and the active filler–polysiloxan-mixture was responsible for this behaviour: The grain boundaries between filler and precursor provide oxygen with an access route into the microstructure while the pure

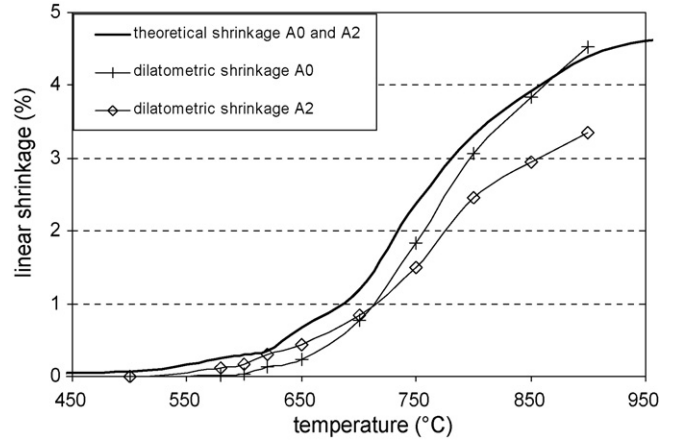

Fig. 4. Comparision between dilatometric shrinkage of specimen A0 and A2 and calculated shrinkage according to Eq. (4a),(4b)(4) during pyrolysis.

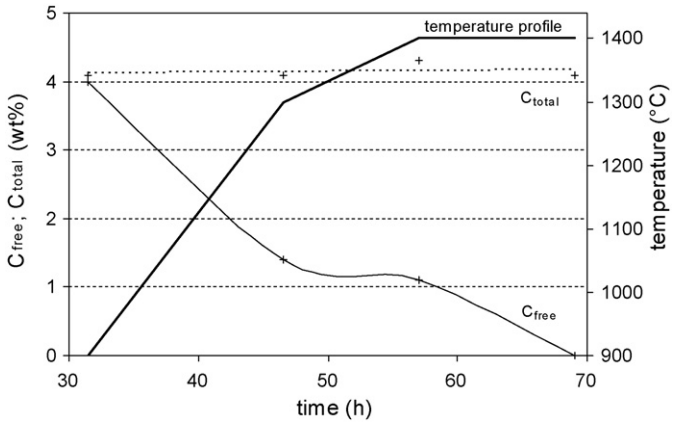

Fig. 6. Changes in free and total carbon amount of specimen A0 during nitridation.

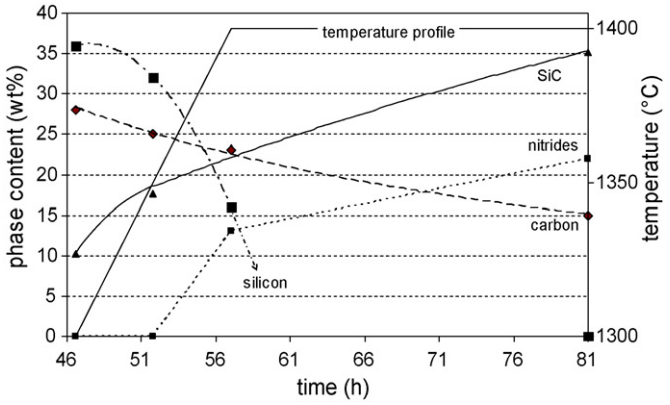

Fig. 7. Development of the phase composition of sample A2 during nitridation.

amorphous precursor provides no path for the oxidising gas to the embedded carbon clusters.

3.3. Nitridation

Further progress in the temperature treatment of the composites leads to a constant decrease in the free carbon content (Fig. 6) while the amount of total carbon remains constant. The changes can be explained by the diffraction pattern of fibreless material (A0) (Fig. 5) which clearly shows SiC formation from the reaction between the free carbon stemming from the precursor and the silicon filler.

As all the examined fibreless and fibre containing composites of the A and B series contain the same amount of polymer, their SiC content formed up to 1300 °C is equal in the range of 10 wt%, as seen for the example of specimen A2 shown in Fig. 7. Increasing the temperature further increases the SiC content until all the carbon provided by the polymer (approximately 4 wt%) is converted to SiC. Therefore a maximum of 13 wt% SiC can be formed (Eq. (1)) from the polymeric carbon and for the fibreless specimen A0 this value is indeed measured after nitridation (Fig. 8). In contrast, an increase in the SiC content beyond this value is observed during nitridation of the fibre-reinforced samples (Fig. 7). The almost linear increase in SiC content with nitridation time can be explained by a reaction

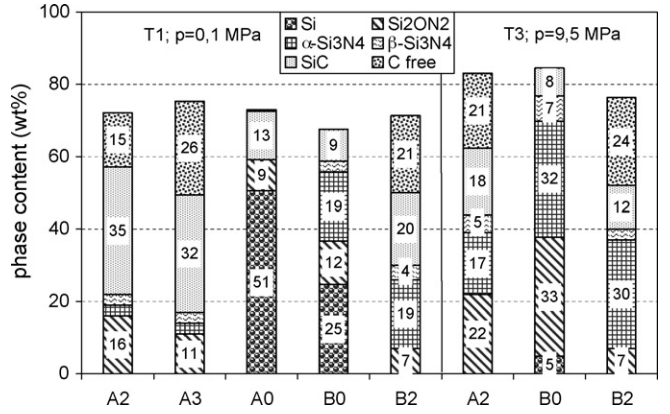

Fig. 8. Phase composition of different composites after nitridation T1 (ambient pressure) and T3 (high pressure, 9.5 MPa).

Table 3
Absolute dimensional change (%) of composites during pyrolysis and nitridation

Specimen	Ambient pressure	High pressure (9.5 MPa)
A0	−5.2	−5.1
B0	−4.8	−5.0
A2	−2.8	−1.7
A3	−3.4	−2.1

between the carbon fibres and the silicon. After nitridation, all the fibre-reinforced specimens contain high SiC amounts due to this reaction (Fig. 8). According to Fig. 7, this reaction starts at about 1340 °C. As this SiC formation causes a volume decrease by 33% ($\rho_{SiC} = 3.2\ g/cm^3$, $\rho_{Si} = 2.3\ g/cm^3$, $\rho_{fibre} = 1.8\ g/cm^3$), development of additional porosity in the range of 10–15 vol% is expected at temperatures above 1300 °C, and this is indeed measured (Fig. 3).

Simultaneous to the formation of SiC, silicon reacts with nitrogen to form nitrides (Figs. 7 and 8). At the onset of nitridation, starting in the temperature range between 1350 and 1400 °C, Si_2ON_2 is the first phase to develop. With increasing nitridation time, more Si_2ON_2 evolves and traces of α- and β-Si_3N_4 are detected. The generation of nitrides and the connected volume expansion does not reduce the porosity and shrinkage of the fibre-containing composites as normally observed for RBSN, Table 3. In fibreless samples, the volume expansion during nitridation closes porosity, resulting in a material with much less porosity than observed in the reinforced samples.

After nitridation, samples A0 and B0 show significant amounts of residual elemental silicon (Fig. 8). Seeding the formation of the nitride with the addition of Si_3N_4 to the starting composition (sample B0) is not sufficient to promote full nitridation of the silicon. Microscopy of cross-sections of fibreless samples shows a densified and fully-reacted nitride shell and a silicon-containing core (Fig. 9). This microstructure is clearly a hindrance to nitridation and explains the high silicon contents observed in fibreless samples.

Increasing the nitridation pressure doubles the amount of nitride phases generated and decreases the SiC content in the

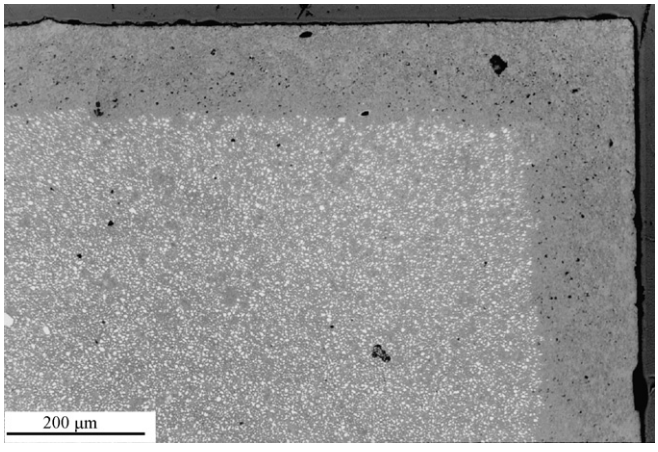

Fig. 9. Cross-section of sample B0 after nitridation T1 (ambient pressure), core – shell structure, white –elemental silicon, grey – nitride phase.

Table 4
Composition of C-fibre reinforced samples after different nitridation

Specimen	Nitridation pressure	fibre/matrix (wt%)	Density matrix (g/cm^3)	fibre/matrix/porosity (wt%)
A2	Ambient (T1)	15/85	2.71	16.2/60.8/23
A3	Ambient (T1)	26/74	2.68	24.7/47.3/28
A2	High (T3)	21/79	3.05	29.2/64.6/6

fibre-reinforced samples (Fig. 8). Furthermore, compared to the material processed at ambient pressure, a higher amount of carbon remains after high pressure nitridation. Volume wise considerations in Table 4 show the significant impact of high pressure on maintaining fibre volume high. This indicates a suppression of fibre attack and explains the reduced SiC content. Around 13 wt%, the amount of SiC found after high pressure nitridation correlates well with the carbon provided by the precursor (Fig. 8). For the fibre-containing samples, pressure nitridation causes a significant reduction in shrinkage due to the improved development of the volume expansive nitride phases, Table 3 and a porosity decrease to 6 vol% (Fig. 3). In contrast, pressure nitridation shows no influence on the total shrinkage and porosity of fibreless samples. However, the core–shell-structure as observed in Fig. 9 is eliminated for sample B0 after nitridation with program T3.

3.4. Mechanical properties of nitrided samples, infiltration

The 3-point bending strength of fibreless composition B0 is 190 ± 15 MPa after high pressure nitridation with program T3 (RT $\rightarrow$ 1170 °C (323 K/h) $\rightarrow$ 1310 °C (28 K/h), 5 h holding, $p_{N_2} = 9.5$ MPa). The fibre containing compositions (A3) have much lower strength of only 43 ± 1 MPa. This difference between the fibreless and fibre-containing materials is caused by cracking along the boundaries between former granules during pyrolysis in the temperature range between 600 and 750 °C.

By infiltrating polysiloxane into the nitrided samples after pyrolysing, the strength of C-fibre reinforced material A3 is only increased slightly to 53 ± 3 MPa after 3 infiltration/pyrolysation steps. The infiltration process lowers the porosity stepwise from the starting porosity of the specimen (Fig. 10). The similar infiltration behaviour of differently nitrided samples with different absolute porosities can be explained by the presence of similar pore architectures in the fibre containing samples (Fig. 11). It also can be concluded from this measurement that pores, particularly down to 0.01 μm, can be closed by the siloxane. The filling of pores is shown in the SEM micrograph in Fig. 12. However, a crack healing in terms of significant strength increase is not caused by siloxane infiltration.

Parallel to the decreasing porosity affected by repeated siloxane infiltration, the *Y*-modulus of the fibre containing

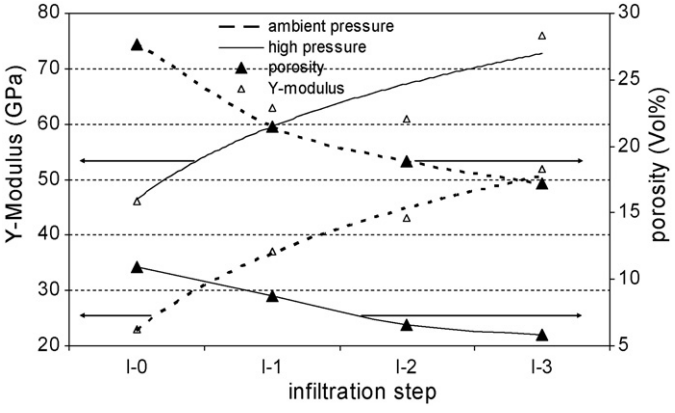

Fig. 10. Development of *Y*-modulus and porosity of composition A3 as a function of the number of polysiloxane infiltration steps after nitridation at ambient and high pressure (I-0 = condition after nitridation).

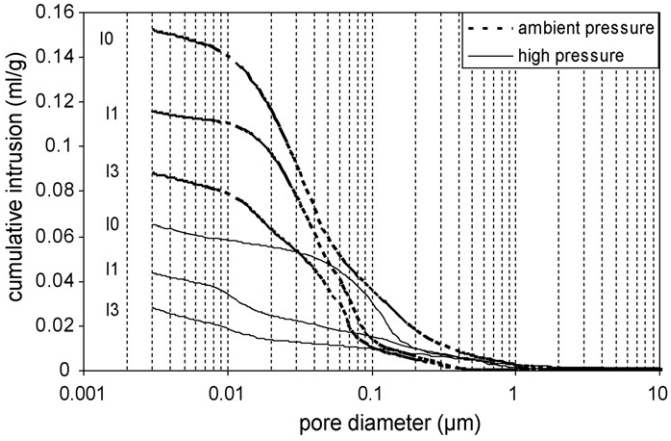

Fig. 11. Changes in pore size distribution of composition A3 due to polysiloxane infiltration (cycle numbers I1-3) after nitridation at ambient and high pressure (I-0).

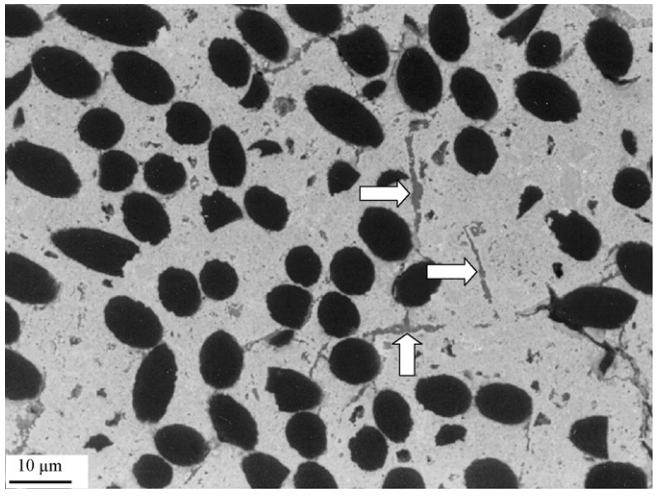

Fig. 12. Cross-section of a polysiloxane-infiltrated fibre-containing specimen (composition A3) after high-pressure nitridation and 3 infiltration steps, pyrolysed up to 1300 °C (BSE backscattered electron image), cracks filled with pyrolysed siloxane (white arrows).

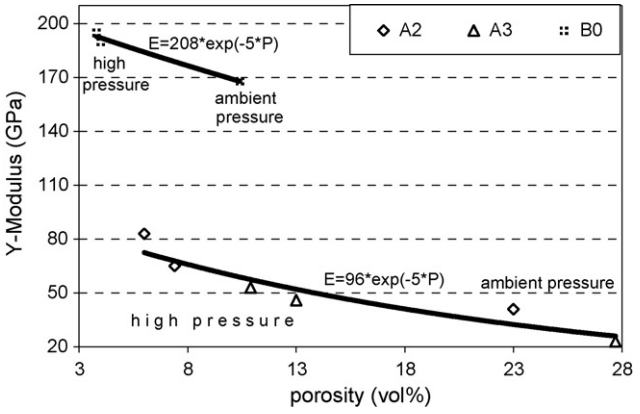

Fig. 13. Young's modulus of C-fibre reinforced (A2 and A3) and fibreless (B0) compositions in relation to different porosities achieved with different nitridation procedures (ambient or high pressure).

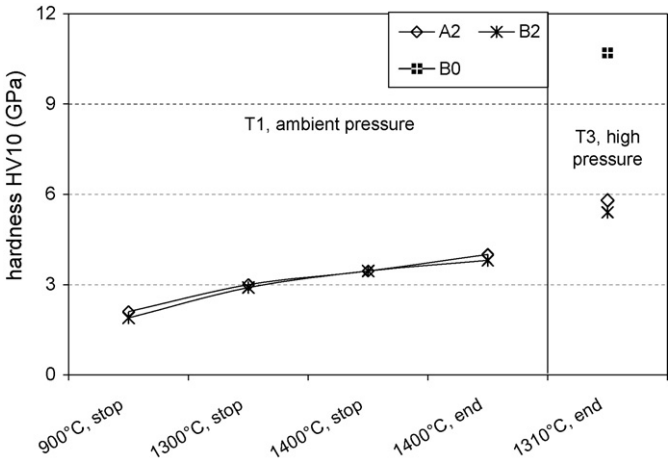

Fig. 14. Evolution of hardness during ambient and high-pressure nitridation.

composition A3 increases gradually and nearly doubles after 3 infiltration/pyrolysation steps (Fig. 10). Parallel and in addition to the densification achieved by siloxane infiltration after nitridation, the nitridation process itself and the porosity and phase composition achieved thereby and the fibre content influences the *Y*-modulus and should therefore be taken into account (Fig. 13). Generally, increasing porosity and fibre volume fraction cause the *Y*-modulus of the different composites to decrease. This effect can be described by the Ryshkewitch-Duckworth equation Eq. (5) in correlation to changing porosity. High pressure nitridation in general leads to a reduced porosity and a higher *Y*-modulus. Zero porosities of samples described can be calculated by Ryshkewitch.

$$E_p = E_0 \exp(kP) \quad (5)$$

P is porosity and *k* is constant (5 for spherical pores).

The nitridation process (Fig. 14) also significantly influences hardness. High pressure nitridation causes the hardness to increase by approximately 30% relative to the material processed at ambient pressure. Significantly less porosity and higher amounts of nitride phases in the material prepared under elevated pressure explain this difference.

3.5. Fibre–matrix interface properties

From the corners of the hardness indentations, cracks propagate into the material. In samples containing C-fibre, crack propagation around fibres is observed which translates into an elongation of the crack path and therefore dissipation of cracking energy. However, this happens only in the quite porous matrix, which results from nitridation at ambient pressure (Fig. 15) left. Furthermore, this pattern of crack propagation is promoted by the separation of the fibre from the matrix caused by the formation of a SiC ring around the C-fibre during processing (Fig. 15) right. Nitridation at high pressure suppresses all SiC formation around the C-fibres, the end results being a much denser matrix. Consequently indentation cracks no longer propagate around the fibres but pass straight through them, as shown in Fig. 16. In all cases where straight crack propagation through fibres is observed, strong fibre-to-matrix bonding can be assumed. Fibre pullout from the fracture surface created by fracture under ten-

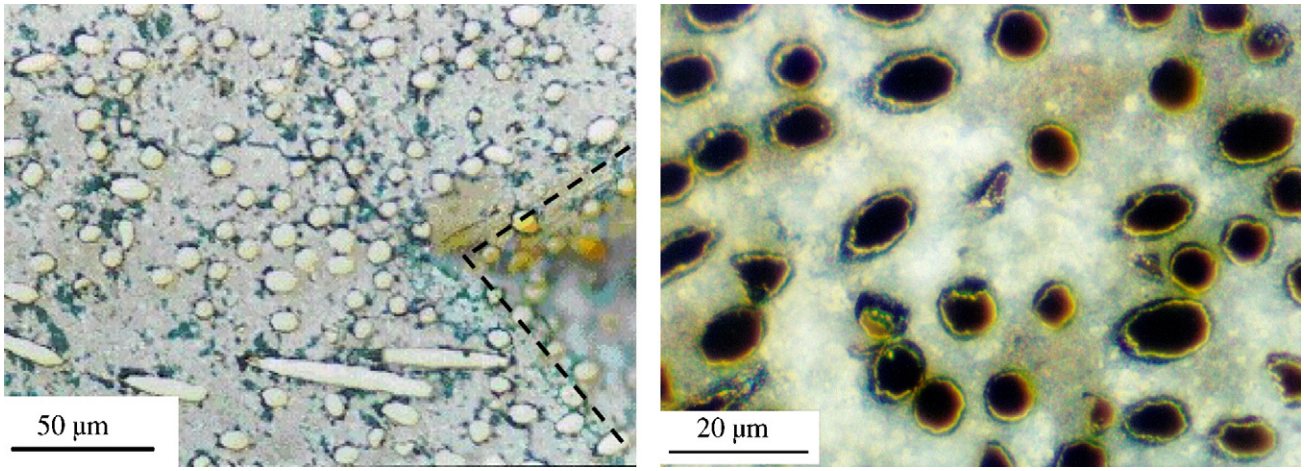

Fig. 15. Cross-section by light microscopy of composition A2 after nitridation at ambient pressure. Left (bright field), crack propagation after hardness indentation (area inside dashed lines). Right (dark field): SiC layer (dark) around a C-fibre (dark) separated by a gap (bright).

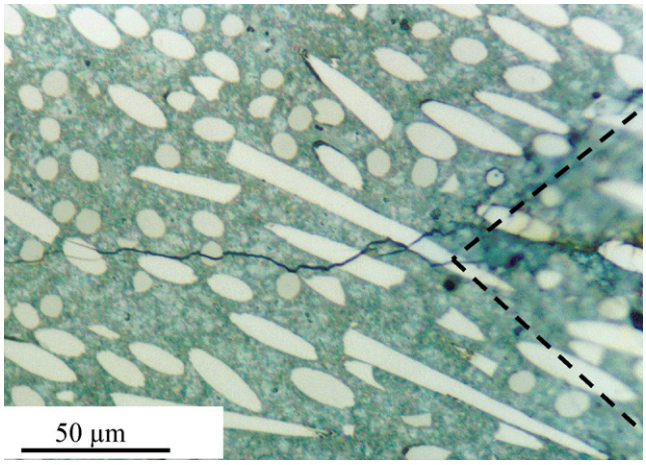

Fig. 16. Cross-section by light microscopy (bright field) of composition B2 after nitridation at high pressure: crack propagation after hardness indentation (area inside dashed lines).

sion, gives evidence for this conclusion: for C fibre reinforced specimens nitrided at high pressure only small or negligible pull-out is found (Fig. 17 right) while specimens nitrided at ambient pressure show clear fibre pullout (Fig. 17 left). In the case of ambient pressure nitridation, the fibre pullout length for C-fibre reinforced samples varies between 10 and 35 μm. Infiltration of these nitrided specimens with polysiloxane also in the gap between fibre and matrix does not change the pullout behaviour significantly, although a significant porosity decrease was shown in Fig. 10. It can be concluded that the siloxane does not promote strong matrix bonding.

4. Discussion

4.1. Fibre shortening

The experimental results showed significant shortening of the fibres during processing. It is well known that sufficient fibre length is vital if short-fibre-reinforced ceramics are to exhibit improved fracture toughness relative to unreinforced ceramics. Within the matrix the fibres have to be long enough to fulfil the demands of the two main energy consuming mechanisms which promote toughening, namely *bridging* of cracks and *pullout* of fibres.[20] The maximum debonding length l_{db} of 101 μm and maximum pullout length l_{po} of 26 μm for carbon fibres in a RBSN matrix can be calculated using Eq. (6)[21] and Eq. (7)[22], respectively:

$$l_{db} = \frac{0.5\sigma_f r}{\tau_g} \tag{6}$$

$$l_{po} = 0.5\left(\frac{r\sigma_f L^{1/m}}{(\tau_g(m+1))}\right)^{m/(m+1)} \tag{7}$$

with $\tau_g = -\mu_g\sigma_{rad}$; $\sigma_{rad} = (E_m E_f)/(E_f(1+\upsilon_m) + E_m(1-\upsilon_f))(\alpha_f - \alpha_m)\Delta T$[23] σ_f is tensile strength 2.5 GPa for C-fibre, r radius fibre 4 μm, τ_g shear stress, L fibre clamping length 25 mm, m Weibull-modulus fibre 5.25, μ_g friction coefficient carbon–RBSN 0.15, σ_{rad} clamping stress 650 MPa for C-fibre, $\upsilon_{f,m}$ transversal contraction 0.25; thermal expansion $\alpha_m = 2.5 \times 10^{-6}$, α_f 8.0×10^{-6} (C-fibre), Young's modulus $E_m = 200$ GPa; $E_f = 230$ GPa, temperature difference $\Delta T = 1107$ K; indices: m—matrix, f—fibre.

Since the measured average length of the C-fibres within the specimens is always greater than 100 μm, the maximum possible increase in fracture toughness may be expected. Therefore the observed fibre shortening does not pose a problem and consequently no changes in the preparation technique of the composite have to be made.

4.2. Packaging and fibre orientation

In general fibres tend to bundle, clump and form textures, in particular if their aspect ratio increases above 25. Consequently fibres longer than the optimum for a particular fibre/matrix combination should be avoided[24]; otherwise severe packing problems such as void formation and anisotropic fibre orientation arise and cause anisotropic and poor composite properties. In contrast very short fibres (aspect ratio < 25) such as the C-fibres in this work (aspect ratio = 15 after kneading) flow and behave like a powder and are much more likely to pack well into a matrix.

However, not only the fibre length has to be taken into account for easy introduction and distribution of fibres in the matrix, density differences between the fibres and the powder matrix,

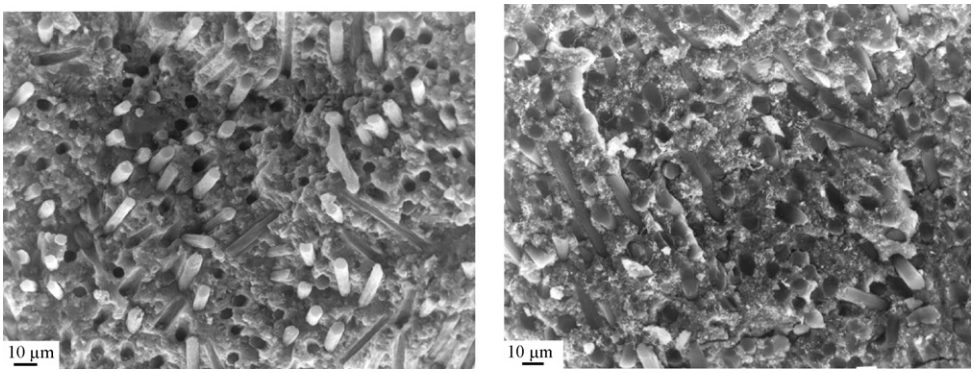

Fig. 17. Fibre pullouts within the fracture surface of a specimen of composition A2. Left: After nitridation at ambient pressure. Right: After nitridation at high pressure.

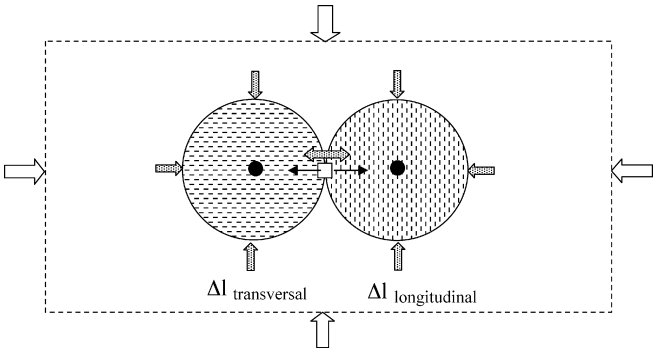

Fig. 18. Differential shrinkage model of granules with perpendicular fibre orientations.

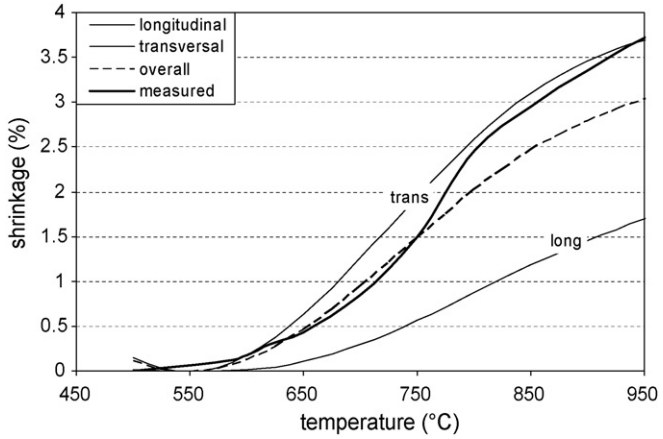

Fig. 19. Calculated shrinkage of granules with different fibre orientations, measured and calculated (overall) composite shrinkage.

which generally lead to separation effects, must also be considered. The tendency for segregation to occur because of density differences can be simply suppressed by the use of a precursor. The high viscosity of the precursor-fibre-powder-mixture during warm mixing at 150 °C makes such separation phenomena impossible. The fibre distribution is only influenced by the shear forces during mixing. When the precursor solidifies during cooling the fibres are fixed within the matrix.

The densifying function of the precursor becomes clear when calculating the packing volume (SV) and porosity of the green composite according to Starr,[25] Eq. (8) for an aspect ratio of 15 with and without precursor. The packing volume of fibres alone has been determined to be SV = 1.5 under slight compression (0.002 MPa). The packing volume of the matrix, composed of silicon and precursor, is always 1.0, regardless of compression applied due to a pore filling function of the siloxane. A pure silicon matrix itself gives a packing volume of 1.8. For composite without precursor, the calculated green state porosity (silicon + fibre) varies as a function of the fibre volume (20–40 vol%) between 20 and 25 vol%. With introduction of the precursor, the calculation points to a fully-dense composite (silicon + fibre + polymer) even at 40 vol% fibre volume, and this is experimentally confirmed (see Fig. 3, polymer state).

$$\mathrm{SV} = \mathrm{SV_p} + (1 - 2\mathrm{SV_p})\Phi + (\mathrm{SV_p} + \mathrm{SV_f} - 1)\Phi^2 \quad (8)$$

Φ—fibre volume, p—particle (matrix), f—fibre, $1/\mathrm{SV} = \rho_{\mathrm{geo}}/\rho_{\mathrm{sceletal}}$.

$$P = 1 - (1/\mathrm{SV})$$

4.3. Differential shrinkage during pyrolysis

During pyrolysis irregular shrinkage of the composites due to precursor shrinkage and different fibre orientations within the granules (Fig. 2) takes place, causing cracking. This effect is called differential shrinkage.[26] The individual shrinkage of each granule can be calculated according to Eq. (9), assuming a model composite as shown in Fig. 18: Aligned fibres, perfect bonding between fibre and matrix, a regular separation distance between the fibres, and elastic behaviour. The calculated overall shrinkage of this simplified composite containing granules with 50% transversal and 50% longitudinal fibre orientation correlates well with the experimental findings (dilatometry) up to 750 °C (Fig. 19). Above 750 °C the measured shrinkage is higher than the calculated composite (overall) shrinkage. The observed deviation from the calculated shrinkage might be explained by differential shrinkage of granules, which influences composite shrinkage. This causes significant stresses between two granules with an ideal perpendicular longitudinal and transversal fibre orientation. The stress can be calculated by Eq. (10).[27]

When the first cracks between granules with different fibre orientation are observed at temperatures around 600 °C, tensile stresses are smaller than 50 MPa.[28] Obviously these stresses are sufficient to cause cracking. Above 750 °C no further crack formation is observed. Above this temperature the measured (dilatometry) and calculated (overall) composite shrinkage deviate significantly up to 0.5% (Fig. 19). The higher measured shrinkage is believed to stem from a viscosity decrease of the precursor at temperatures above 750 °C, which enhances the shrinkage rate. Consequently a relaxation of the internal stresses built up by differential shrinkage takes place and further cracking is prevented. In the same temperature range of 750 °C Seibold[12] postulated a viscosity decrease for a polysiloxane precursor based on exothermic DTA measurements.

$$\varepsilon_{\mathrm{l}} = \frac{\varepsilon_{\mathrm{m}} E_{\mathrm{m}} V_{\mathrm{m}} + \varepsilon_{\mathrm{f}} E_{\mathrm{f}} V_{\mathrm{f}}}{E_{\mathrm{m}} V_{\mathrm{m}} + E_{\mathrm{f}} V_{\mathrm{f}}} \quad \text{longitudinal (parallel to the fibre)} \quad (9a)$$

$$\varepsilon_{\mathrm{t}} = (1 + \upsilon_{\mathrm{m}})\varepsilon_{\mathrm{m}} V_{\mathrm{m}} + \varepsilon_{\mathrm{f}} V_{\mathrm{f}}$$

transversal (perpendicular to the fibre) (9b)

$$\varepsilon_{\mathrm{ges}} = \frac{\varepsilon_{\mathrm{l}} + 2\varepsilon_{\mathrm{t}}}{3} \quad \text{overall} \quad (9c)$$

$$\sigma_{\max} = (\varepsilon_{\mathrm{t}} - \varepsilon_{\mathrm{l}})\frac{E_{\mathrm{m}}}{2(1 - \nu)} \quad (10)$$

ε is shrinkage: $\varepsilon_{\mathrm{f}} = 0$, $\varepsilon_{\mathrm{m,500–600°C}} = 0.05\%$, $\varepsilon_{\mathrm{m,500–750°C}} = 1.84\%$; Young's modulus: $E_{\mathrm{m}} = 200$ GPa, $E_{\mathrm{f}} = 200$ GPa; V volume parts, ν transversal contraction = 0.25, σ strength, indices: l—longitudinal, t—transversal, m—matrix, f—fibre.

4.4. Mechanical properties, toughening

In consequence of cracking mechanical characterisation of the fibre reinforced polymer modified RBSN is difficult and the application potential of this material with focus of quasiductility is speculative. According to Becher[20] main contributors to fracture toughness are fibre pullout, bridging and crack deflection which all were observed in the experiments. To overcome the cracking problems efforts should be made to minimise in particular the problem of differential shrinkage of areas of oriented fibres (domains). Application of an interface between fibre and matrix might be a solution: A weak interface causes relaxation of internal stresses between fibre and matrix and finally causes homogeneous shrinkage of domains independent of fibre orientation. Chih and Fu[29] controlled such stress relaxation in a CMC by a silica interface. They postulated minimised internal stresses between fibre and matrix allowing unhindered shrinkage and finally decreasing the differential shrinkage and avoiding cracking. Another more difficult solution of the cracking might be the general avoidance of different fibre orientation in the CMC. One way of reducing the orientation is by decreasing the size of the granules causing a more homogenous composite in a macroscopic scale minimising cracking by domain orientation. However, the more intensive the granulation the more intensive the fibre shortening which finally lowers fibre length and limits therefore its toughness contribution. Another approach might be the application of more sensitive preparation methods, which avoid fibre shortening and orientation.

4.5. Nitridation, effect of siloxane and Si_3N_4 seeding

After heating up to 900 °C, 5 vol% and 1 vol% porosity, respectively, were measured in the fibre containing and fibreless specimens. Upon nitridation up to 1300 °C, a significant increase in porosity into the range of 10 vol% was detected. Since up to this temperature the SiC formation reaction between elemental silicon and carbon fibre which is associated with a volume decrease is not observed, this increase in porosity can be explained by SiO formation by reaction between SiO_2 of the devitrified SiOC-glass and the elemental silicon, Eq. (11). Furthermore, Erny[15] identified structural changes during devitrification of SiOC-glasses, mainly the opening of closed porosity, as a source of porosity increase. A further source of porosity might be the carbothermal reduction reaction between the C-fibres and SiO_2 stemming also from the devitrified polymer. CO detected in the furnace atmosphere at 1380 °C points to this reaction mechanism, Eq. (12).

$$SiO_2(s) + Si(s) \rightarrow 2SiO(g) \quad (11)$$

$$SiO_2(s) + 2C(s) \rightarrow SiC(s) + CO(g) \quad (12)$$

Besides the creation of porosity, SiO developing according to Eq. (11) has to be taken into account for nitridation. As the elemental silicon particles are covered by the devitrified precursor, a SiO_2-barrier effect has to be regarded. According to Marcks,[30] the partial pressure of SiO, evolved by Eq. (11), is large enough at temperatures above 1250 °C to penetrate outwards through the silica barrier. The layer thickness and the viscosity, which is determined by the chemical composition of the barrier, both have an influence on the sealing effect of the barrier. Generally speaking as both values increase, the SiO release temperature increases as well. Since nitrogen-containing phases are found in the specimens at temperatures above 1350 °C, a release of SiO above this temperature seems likely. Consequently the nitridation reaction Eq. (13) is dominant at the onset of nitridation. The process of direct nitridation of silicon starting even below 1250 °C as postulated by Pigeon and Varma[31] is suppressed by the presence of silica in the composite system. Similar observations of nitridation hindrance of silicon by preceramic polymer residues were made by Mohr et al.[32] during nitridation of a whisker-reinforced silicon/silazane mixture.

$$SiO_2(s) + 3Si(s) + 2N_2(g) \rightarrow 2Si_2ON_2(s) \quad (13)$$

Further increases in temperature above 1350 °C cause an increase in the partial pressure of SiO and allows formation of α-Si_3N_4 via a gas-phase reaction. At higher temperatures formation of β-Si_3N_4 by direct nitridation is also possible and proven by XRD measurement.

The differences in porosity developed below the nitridation temperature ($T > 1350$ °C) which stem from the different specimen starting compositions explain the significant differences in the subsequent nitridation behaviour of the fibreless and fibre-containing specimens found by XRD examination (Fig. 8). According to Pigeon et al.,[33] nitridation is controlled by free diffusion ($D_{eff} > 10^{-2}$ cm^2/s) of the gas phase accompanied by Knudson diffusion ($D_{eff} = 10^{-5}$–10^{-2} cm^2/s). A pore size and porosity decrease due to volume expansion changes the diffusion mechanism from free diffusion towards the less effective Knudson process. This can be observed well in samples A0 and B0 when porosity decreases during nitridation (Fig. 3) and nitridation stops while elemental silicon is still present in significant amounts. For the fibre containing specimens, a gradual progress in nitridation is observed in Fig. 7 until all the elemental silicon is transformed. The increasing porosity due to parallel formation of SiC by reaction between C-fibres and elemental silicon supports the free diffusion mechanism of nitrogen and therefore promotes nitridation. However, this reaction between silicon and carbon to form the carbide is not desired as it consumes reinforcing fibres.

The SiC formation by the aforementioned reaction can be suppressed by increasing the nitrogen pressure. Wada et al.[34] postulated a 100 °C decrease in the formation temperature of Si_3N_4 and Si_2ON_2 when the nitrogen pressure increases from 0.1 to 1 MPa. Indeed it is observed that when the nitrogen pressure is increased from 0.1 to 9.5 MPa, the temperature of the onset of nitridation was lowered in the experiment from 1350 to 1250 °C. Greil[4] explains this improvement in nitridation behaviour of precursor ceramics by stabilisation of an open pore channel system in the precursor at higher pressures which allows improved gas transport and therefore nitridation. Consequently the nitridation result for fibreless samples is also improved by pressure increase.

Nitridation of the specimens can be also improved and accelerated by Si_3N_4 dilution of the matrix, as shown here in the B-series. This causes a so-called seeding effect[35,36] which elim-

inates the rate determining nucleation step during the nitridation reaction. However, full nitridation of B0 at ambient pressure is still impossible and 9.5 MPa N_2 pressure is needed to achieve practically full nitridation.

5. Conclusion

The advantageous and disadvantageous effects of using preceramic polymer in the process demonstrated are numerous and can be divided into effects specific to the shaping (polymer state) and pyrolysis/nitridation states.

(1) Shaping (polymer state)
- The use of a meltable polymer allows the use of polymer-related technologies for shaping such as injection moulding and warm pressing.
- The precursor enables the introduction of high volumes and isotropic distributions of fibres in a ceramic matrix. Since the porosity of the achieved specimens is very low, a pore-filling function of the precursor is obvious.

(2) Pyrolysis/nitridation
- High volume shrinkage of the polymer during pyrolysis causes cracking between domain-like areas of different fibre orientations.
- Viscous flow of the precursor above 750 °C stops cracking and is responsible for shrinkage and low porosities (1–4 vol%) of specimens processed up to 900 °C.
- Porosity in the precursor/silicon mixtures is formed by reaction between devitrified precursor and silicon.
- Pyrolysis products of the precursor form a SiOC-glass barrier, which hinders nitrogen diffusion and postpones formation of nitride phases to temperatures above 1350 °C. This encourages the reaction between silicon and C-fibres which forms SiC and significantly increases the porosity of fibre composites. A high nitrogen pressure supports nitridation and suppresses SiC formation and promotes the formation of a denser composite.
- Silica devitrification products from the precursor can be nitrided and preferentially form Si_2ON_2.

Assessment of the properties of the new CMC mainly lack the impossibility to measure the fracture toughness due to the cracking in consequence of differential shrinkage. Increased quasi-ductility, and therefore fracture toughness, is one of the main goals of fibre reinforced ceramics which was not reached here. The measurable properties of the new CMC and polymer modified RBSN (PMRBSN) matrix material are summarised in Table 5 and the improved properties of PMRBSN in comparison to conventional RBSN should be emphasized.

Based on the ease of processing, shapeabililty by injection molding, machinabilty in the polymer and pre-nitrided state and the absence of shrinkage, cost-effective near-net-shape manufacturing of complex ceramic parts is possible with this new method. A transfer of the technique of polymer modification and/or fibre reinforcement to ceramic materials other than nitride ceramics seems promising and generally possible. Generally speaking the technique introduced here opens new horizons for production on an industrial scale of complex parts for the machine industry and substrates for functional ceramics. Particularly the high potential of the material for long-term high-temperature applications makes it interesting for energy technology.

Table 5
Properties of polymer-modified fibreless and fibre-reinforced RBSN

	C_f/PMRBSN	PMRBSN	RBSN
Fibre (vol%)	20–40	0	0
Microstructure			
Density (g/cm^3)	2.3–2.4	2.7–3.0	2.5
Porosity (%)	4.0–11.0	3.0–8.0	10.0–20.0
Mechanical properties			
Bending strength (3-pt., MPa)	50	200	200
E-Modul (GPa)	50–80	200	200
Hardness, HV10	6	11	10[a]
Thermal parameters			
Thermal expansion (up to 1400 °C)	3.2–3.9	3.8	3.2

[a] According to http://www.azom.com/details.asp?ArticleID=77.

References

1. Benitsch, B., Carbon fibre based silicon carbide ceramics for industrial applications. *cfi/Ber. DKG*, 2005, **82**(9), E44–E46.
2. Krenkel, W., Heidenreich, B. and Renz, R., C/C-SiC composites for advanced friction systems. *Adv. Eng. Mater.*, 2002, **4**(7), 427–436.
3. Kevorkijan, V., Ceramic break rotor for passenger cars. *Am. Ceram. Soc. Bull.*, 2002, **81**(4), 27–29.
4. Greil, P., Active filler controlled pyrolysis of preceramic polymers. *5th Proc. Eur. Ceram. Soc.*, 1995, **4**, 101ff.
5. Herzog A., Manufacturing and properties of short fibre reinforced reaction bonded silicon nitride, (Herstellung und Eigenschaften von reaktionsgebundenem Siliciumnitrid). PhD thesis. University Erlangen-Nuernberg, VDI Fortschrittsberichte Reihe 5 Nr. 668, VDI Verlag, Düsseldorf, Germany, 2002 (in German only).
6. Krautkrämer, H., *Werkstoffprüfung mit Ultraschall*. Springer Verlag, Berlin, 1966.
7. O'Conner, J. E., Short-fiber-reinforced elastomer composites. *Rubber Chem. Technol.*, 1977, **50**, 945–958.
8. Bader, M. and Hill, A., Short fiber composites. In *Materials Science and Technology*, ed. R. Cahn, P. Haasen and E. Kramer. Wiley-VCH, Weinheim, 1993, p. 327.
9. Eduljee, R. and McCullough, R., Elastic properties of composites. In *Materials Science and Technology*, ed. R. Cahn, P. Haasen and E. Kramer. Wiley-VCH, Weinheim, 1993, p. 393.
10. Renlund, G., Prochazka, S. and Doremus, R., Silicon oxycarbid glasses, I + II. *J. Mater. Res.*, 1991, **6**(12), 2716ff.
11. Hurwitz, F., Heimann, P., Gyekenyesi, J., Masnovi, J. and Bu, X., Polymeric routes to silicon carbide and silicon oxycarbide. *Ceram. Eng. Sci. Proc.*, 1991, **12**, 1292ff.
12. Seibold, M., Filler induced reaction pyrolysis of polymeric precursors a new concept for production of ceramic composites (Füllergesteuerte Reaktionspyrolyse polymerer Precursoren - ein neues Verfahren zur Herstellung keramischer Verbundwerkstoffe). PhD thesis. University Erlangen-Nuernberg, VDI Fortschrittsberichte Reihe 5, VDI Verlag, Düsseldorf, Germany, 1993 (in German only).
13. Hurwitz, F., Heimann, P., Farmer, S. and Hembree, D., Characterisation of pyrolytic conversion of polysilsesquioxanes to silicon oxycarbide. *J. Mater. Sci.*, 1993, **28**, 6622ff.
14. Bois, L., Maquet, J. and Babouneau, F., Structural characterisation of sol–gel derived oxycarbide glasses. *Chem. Mater.*, 1995, **7**, 975ff.

15. Erny, T., Production, structure and properties of polymer derrived composites in the MeSi/Polysiloxane system (Herstellung, Aufbau und Eigenschaften Polymer abgeleiteter Verbundkeramik des Ausgangssystems MeSi/Polysiloxan). PhD thesis. University Erlangen-Nuernberg, VDI Fortschrittsberichte Reihe 5, VDI Verlag, Düsseldorf, Germany, 1996 (in German only).
16. Greil, P. and Seibold, M., Modelling of dimensional changes during polymer ceramic conversion for bulk component fabrication. *J. Mater. Sci.*, 1992, **27**, 1053ff.
17. Erny, T., Seibold, M., Jarchow, O. and Greil, P., Microstructure development of oxycarbide composites during active-filler-controlled polymer pyrolysis. *J. Am. Ceram. Soc.*, 1993, **76**(1), 207ff.
18. Burns, G., Taylor, R., Zu, Y., Zangvil, A. and Zank, G., High temperature chemistry of the conversion of siloxanes to silicon carbide. *Chem. Mater.*, 1992, **4**, 1313ff.
19. Müller, C., A new oxidation protection system for porous ceramics derived from filled silicon polymers (Neuartige Oxidationsschutzbeschichtungen für poröse Keramiken ausgehend von gefülltem Silicium-Polymer). PhD thesis. University Erlangen-Nuernberg, VDI Fortschrittsberichte Reihe 5 Nr. 545, VDI Verlag, Düsseldorf, Germany, 1999 (in German only).
20. Becher, P., Microstructural design of toughend ceramics. *J. Am. Ceram. Soc.*, 1991, **74**(2), 255ff.
21. Kelly, A. and Tyson, W., Tensile properties of fibre reinforced metals. *J. Mech. Phys. Solids*, 1965, **13**, 329ff.
22. Navarre, G., Etude des mecanismes d'endommagement et de rupture des materiaux composites a fibres et a matrice ceramiques. PhD thesis. Institut National des Siences Appliquees de Lyon, France, 1990.
23. Rosen, B., Thermomechanical properties of fibrous composites. In *Proceedings of the Royal Society of London A 319*. Materials Science Corporation, Washington, PA, 1970, p. 79ff.
24. Milewski, J., Efficient use of whiskers in the reinforcement of ceramics. *Adv. Ceram. Mater.*, 1986, **1**(1), 36ff.
25. Starr, T., Packing density of fiber/powder blends. *Am. Ceram. Soc. Bul.*, 1986, **65**(9), 1293ff.
26. Schapery, R., Thermal expansion coefficients of composite materials based on energy principles. *J. Comp. Mater.*, 1986, 380ff.
27. Munz, D. and Fett, T., *Mechanical Behaviour of Ceramic Materials (Mechanisches Verhalten Keramischer Werkstoffe)*. Springer Verlag, Berlin, 1989 (in German only).
28. Herzog, A., Vogt, U. and Woetting, G., Short fibre reinforced RBSN. 7th Conference and Exhibition of the European Ceramic Society. *Key Eng. Mater.*, 2002, **206**(2), 923–928.
29. Chih, C.-C. and Fu, S.-Y., Effects of amorphous silica coatings on the sintering behaviours of SiC whisker reinforced Al_2O_3 composites. *J. Mater. Sci.*, 1994, **29**(12), 3215ff.
30. Marcks, A., Influence of oxygen to the nitirdation kinetics of silicon (Einfluss von Sauerstoff auf die Nitridierungskinetik von Silicium). PhD thesis. Technische Universität Berlin, Germany, 1980 (in German only).
31. Pigeon, R. and Varma, A., Quantitative kinetic analysis of silicon nitridation. *J. Mater. Sci.*, 1993, **28**, 2999ff.
32. Mohr, D., Desai, P. and Starr, T., Production of Si_3N_4/SiC fibrous composites using polysilazanes as pre-ceramic binders. *Ceram. Eng. Sci. Proc.*, 1990, **11**(7–8), 920ff.
33. Pigeon, R., Varma, A. and Miller, A., Some factors influencing the formation of reaction bonded silicon nitride. *J. Mater. Sci.*, 1993, **28**, 1919ff.
34. Wada, H., Ming, W. and Tseng, T., Stability of phases in the Si–C–N–O system. *J. Am. Ceram. Soc.*, 1988, **71**(10), 37ff.
35. Licko, T., Figusch, V. and Puchyova, J., Synthesis of silicon nitride by carbothermal reduction and nitriding of silica: control of kinetics and morphology. *J. Eur. Ceram. Soc.*, 1992, **9**(3), 219ff.
36. Weimer, A., Eisman, G., Susnitzky, D., Beaman, D. and McCoy, J., Mechanism and kinetics of carbothermal nitridation synthesis of alpha-silicon nitride. *J. Am. Ceram. Soc.*, 1997, **80**(11), 2853ff.